

1 **An open-hardware platform for optogenetics and photobiology**

2
3 Karl P. Gerhardt¹, Evan J. Olson², Sebastian M. Castillo-Hair¹, Lucas A. Hartsough¹,
4 Brian P. Landry¹, Felix Ekness³, Rayka Yokoo⁵, Eric J. Gomez¹, Prabha
5 Ramakrishnan¹, Junghae Suh^{1,3}, David F. Savage^{5,6}, Jeffrey J. Tabor^{1,3,4*}.

6
7 ¹Department of Bioengineering, ²Graduate Program in Applied Physics, ³Systems,
8 Synthetic, and Physical Biology (SSPB) Ph.D. Program, ⁴Department of Biosciences,
9 Rice University, Houston, Texas, 77005, USA

10
11 ⁵Department of Molecular & Cell Biology, ⁶Department of Chemistry, University of
12 California, Berkeley, Berkeley, CA, 94720, USA

13 *Contact: jeff.tabor@rice.edu

16 **Abstract**

17 In optogenetics, researchers use light and genetically encoded photoreceptors to
18 control biological processes with unmatched precision. However, outside of
19 neuroscience, the impact of optogenetics has been limited by a lack of user-friendly,
20 flexible, accessible hardware. Here, we engineer the Light Plate Apparatus (LPA), a
21 device that can deliver two independent 310 to 1550 nm light signals to each well of a 24-
22 well plate with intensity control over three orders of magnitude and millisecond resolution.
23 Signals are programmed using an intuitive web tool named Iris. All components can be

24 purchased for under \$400 and the device can be assembled and calibrated by a non-
25 expert in one day. We use the LPA to precisely control gene expression from blue, green,
26 and red light responsive optogenetic tools in bacteria, yeast, and mammalian cells and
27 simplify the entrainment of cyanobacterial circadian rhythm. The LPA dramatically
28 reduces the entry barrier to optogenetics and photobiology experiments.

29

30

31 In 2005, Deisseroth and co-workers reported the expression of a blue light
32 activated microbial ion channel (opsin) in mammalian neurons and its use for
33 physiologically-relevant, millisecond timescale optical control of neural activity *in vitro*¹.
34 However, because no instrument existed for delivering the necessary intensity of light to
35 specific brain regions in live animals without major side effects, optogenetics contributed
36 few neurobiological insights between 2005 and 2009². During this period, the group
37 engineered the optical neural interface (ONI) – a brain-implantable optical fiber with a
38 laser diode light source. By combining the ONI with microbial opsins, they achieved
39 optogenetic control of rat motor behavior³ and identified neural activity patterns that cause
40 sleeping mice to wake⁴. The ONI was rapidly adopted by the greater community and
41 combined with opsins and other photoreceptors, resulting in a wave of breakthroughs in
42 a short time period².

43 Following Quail and co-workers' pioneering engineering of a red/far red light-
44 switchable *S. cerevisiae* transcriptional regulatory (promoter) system in 2002⁵,
45 photoreceptors with diverse spectral properties have been used to control a remarkable
46 range of cell biological processes in mechanistically tractable model organisms as well.
47 For example, light-switchable promoter systems have been engineered in *E. coli*⁶⁻¹¹,

48 cyanobacteria¹², yeast^{13,14}, mammalian cells^{15–24}, fruit flies²⁵, zebrafish^{21,26} and plants²⁷.
49 Translation^{28,29}, proteolysis³⁰, membrane recruitment^{13,31}, signaling^{31–39}, ER-to-
50 cytoplasm⁴⁰ and nuclear^{41–44} translocation, and genome editing^{13,45,46} have also been
51 placed under optogenetic control.

52 However, no optical hardware has been developed to enable the broad research
53 community to properly utilize these non-neural optogenetic tools, limiting their impact. For
54 example, we recently engineered the Light Tube Array (LTA), a light emitting diode (LED)-
55 based device that exposes 64 shaking incubated culture tubes to programmable light
56 signals with an intensity range over three orders of magnitude and millisecond
57 resolution⁴⁷. Though the LTA enables unrivaled control of gene expression dynamics⁴⁷,
58 construction requires custom machined components, specialized assembly tools, and
59 knowledge of electronic system design and programming is done in computer language.
60 Additionally, experiments are not scalable due to the large instrument size (0.02 m³) and
61 requirement for connection to an external computer. Furthermore, the tubes are costly
62 (~\$0.10/each) and restrict experiments to suspension culture organisms such as bacteria
63 and yeast. Finally, the LEDs are permanently soldered, limiting optical flexibility. In
64 another example, Moglich and coworkers modified the injection port of a Tecan microplate
65 reader with an optical fiber and eight LEDs from 385 – 850 nm⁴⁸. While this clever design
66 enables programmable sample illumination via the commercial software, the Tecan
67 instrument costs ~\$40,000. Other recent designs^{35,42,49–52} suffer various limitations and
68 have not found widespread adoption.

69 We have designed the LPA for compatibility with a wide range of optogenetics and
70 photobiology experiments and model organisms, low device and consumable costs, high

71 scalability and throughput, and accessibility by laboratories without hardware expertise.
72 We demonstrate its capabilities by recapitulating and extending our LTA results in *E. coli*,
73 performing yeast and mammalian optogenetic gene expression control experiments, and
74 easing the entrainment of cyanobacterial circadian rhythm. Additionally, because the LPA
75 and Iris are open source, they may be freely modified and extended by the community for
76 additional functionalities.

77

78 **Results**

79 LPA design and assembly

80 The core of the LPA is a printed circuit board (PCB) (**Supplementary Fig. 1a-c**)
81 outfitted with a Secure Digital (SD) card reader (**Supplementary Figs. 1c and 2**), an
82 Atmel ATmega328a microcontroller (**Supplementary Figs. 1c and 3**), 3 LED drivers
83 (**Supplementary Figs. 1c and 4**), 48 solder-free LED sockets (**Supplementary Fig. 1a**),
84 a power regulating circuit (**Supplementary Fig. 5**), and other standard electronics
85 components (**Supplementary Table 1**). The only external connection is to a 5v power
86 supply (**Fig. 1a and Supplementary Fig. 6**). The unpopulated PCB can be ordered from
87 a commercial supplier using the provided fabrication files (**Supplementary Information**).
88 The PCB can be assembled (populated with electronic components) via do-it-yourself
89 (DIY) (**Supplementary Procedure 1 and Supplementary Table 2**) or commercial
90 (**Supplementary Procedure 1**) soldering procedures. We recommend DIY installation of
91 the LED sockets using a 3D printed socket alignment tool (**Supplementary Fig. 7a and**
92 **Supplementary Procedure 1**) to ensure consistent geometries and illumination across

93 the wells. We have provided a video tutorial demonstrating PCB assembly
94 **(Supplementary Video 1)**.

95 The microcontroller converts an Iris-generated file stored on the SD card to LED driver
96 control signals. Each LED driver individually regulates the intensity of 16 LEDs over 4096
97 levels with a 1 ms refresh rate via 12-bit pulse width modulation of output current up to
98 20 mA. The output of each driver, and thus LED intensity, can be further controlled with
99 6-bit resolution by adjusting dot correction settings in the device's firmware
100 **(Supplementary Figs. 8-14, Supplementary Tables 3 and 4, Supplementary**
101 **Procedures 2 and 3, and Supplementary Note 1)**.

102 Each socket secures a 5 mm through-hole LED via a friction fit **(Supplementary Fig.**
103 **15)**. These LEDs are commercially available with wavelengths from 310 to 1550 nm
104 **(Supplementary Table 5)**, enabling plug-and-play optical reconfiguration
105 **(Supplementary Procedure 4)**. The 20 mA driver output permits full range control of
106 most 5 mm LEDs.

107 A 3D printed chassis houses the assembled PCB and 24-well plate **(Fig. 1a-c)**.
108 The chassis comprises i) a mounting plate, ii) LED spacer, iii) plate adapter, and iv) plate
109 lid **(Supplementary Fig. 16a-d)**. We have designed 4 mounting plates, ensuring
110 compatibility with most shaker platforms **(Supplementary Information)**. The mounting
111 plates contain recessed holes **(Fig. 1c and Supplementary Fig. 16a)** for upward-facing
112 bolts that align and stack the remaining 3 modules. The LED spacer **(Supplementary**
113 **Fig. 16b)** creates a fixed distance between each LED socket pair and overhead well, and
114 optical isolation between wells. The spacer is mated with the PCB and the resulting
115 assembly stacked atop the mounting plate. The plate adapter **(Supplementary Fig. 16c)**

116 is placed atop the spacer. A black-walled, transparent plastic bottomed 24 well plate
117 (**Supplementary Fig. 17** and **Supplementary Table 6**) is aligned and held in place by
118 the plate adapter. An adhesive foil plate cover (**Supplementary Table 6**) provides a
119 sealed environment for each well. Laser cut nitrile gaskets (**Supplementary Fig. 18** and
120 **Supplementary Procedure 5**) are placed at each of the 3 interfaces above the PCB to
121 reduce optical contamination. Finally, the lid (**Supplementary Fig. 16d**) is placed atop
122 the plate and the complete assembly is secured with wing nuts (**Fig. 1b** and
123 **Supplementary Table 6**). All chassis modules can be 3D printed using supplied files
124 (**Supplementary Information, Supporting Procedure 6**). We have provided a written
125 procedure and instructional video demonstrating LPA assembly (**Supplementary**
126 **Procedure 7** and **Supplementary Video 2**).

127

128 LPA programming with Iris

129 Iris can be freely accessed at <http://iris.taborlab.rice.edu> or run locally using the
130 provided source code (**Supplementary Note 2**). Light programs are specified in Steady
131 State, Dynamic, or Advanced Modes (SSM, DM, AM). In SSM, time-invariant intensities
132 for each LED are entered within an Input Panel (**Fig. 2a, left**). In DM, constant, step,
133 sinusoidal, or piecewise light signals are specified using parameters such as initial and
134 final intensity, time of step, or wave period, amplitude, and offset (**Supplementary Note**
135 **3**). The same signal is run by all 24 top LEDs, and the same, or a second signal can be
136 run by all 24 bottom LEDs. AM (**Fig. 2b, left**) implements DM signals via our recent
137 staggered-start protocol, which allows kinetic experiments to be performed with far less
138 sample handling⁴⁷ (**Supplementary Fig. 19, Supplementary Table 7**). The light signal

139 run in each well can be randomized (**Supplementary Note 4**) to mitigate any well-to-well
140 variability. We have provided videos demonstrating Iris light signal programming in all 3
141 modes (**Supplementary Videos 3-5**).

142 Light programs can be viewed and debugged at the plate (**Fig. 2a, right**) or
143 individual well (**Fig. 2b, right**) levels using the Simulation Panel. When the program is
144 satisfactory, the download button (**Fig. 2a,b**) is pressed. Iris then generates i) a device-
145 readable binary file (.lpf, **Supplementary Table 8**) used to run the LPA, ii) a session file
146 for reloading a program into Iris at a later time, and iii) a CSV file containing user-readable
147 well randomization information in a zip folder. The .lpf is then transferred to an SD card,
148 which is inserted into the LPA, and the Reset Button (**Supplementary Fig. 1a**) is pressed
149 to run the light program. Included Python scripts can be used to automate .lpf design
150 (**Supplementary Information, Supplementary Note 5**), increasing throughput.

151

152 LPA calibration

153 We have developed a simple method utilizing a gel imager and MATLAB script to
154 calibrate the outputs of multiple LPA LEDs of one spectrum to one another
155 (**Supplementary Information, Supplementary Procedure 8**). To calibrate absolute
156 outputs, or the outputs of LEDs with different spectra, we have developed a method
157 combining a probe spectrophotometer and 3D printed adapter that fits the LPA wells
158 (**Supplementary Figs. 6b, 20 and Supplementary Procedure 8**). Using either method,
159 outputs are adjusted by loading two manually generated text files specifying the grayscale
160 and dot correction values for each LED (**Supplementary Procedure 8**, examples in

161 **Supplementary Information**) on to the SD card before running an experiment.
162 Calibration typically reduces LEDs output variability to <1% (**Supplementary Fig. 21**).

163

164 Benchmarking the LPA with *E. coli* CcaS-CcaR.

165 CcaS-CcaR is a green light activated, red de-activated two component system
166 (TCS) that we previously engineered to control gene expression in *E. coli* (**Fig. 3a**)⁸. Using
167 the LTA and a superfolder GFP (sfGFP) output, we characterized the relationship
168 between green and red light inputs and transcriptional output dynamics (i.e. I/O)⁴⁷. We
169 developed a predictive mathematical model of the I/O, which we used to pre-compute
170 green light time courses to drive CcaS-CcaR output to follow tailor-made (reference) gene
171 expression signals with high predictability⁴⁷.

172 We aimed to benchmark the LPA by repeating these CcaS-CcaR experiments.
173 First, we measured the steady state response to green light intensity by outfitting the
174 bottom positions of an LPA with 533 nm (green) LEDs and programming them to emit
175 between 0.00 and 20.10 $\mu\text{mol m}^{-2} \text{s}^{-1}$ photons. We grew our previous strain in a shaking
176 LPA under these conditions and measured sfGFP output using flow cytometry (**Methods**).
177 We observed that sfGFP increases sigmoidally with green intensity with a 5.3-fold
178 dynamic range and Hill parameter (n_H) = 2.6 (**Fig. 3b**), tightly consistent with LTA
179 measurements. The intensity resulting in half maximal output ($k_{1/2}$) is 0.22 $\mu\text{mol m}^{-2} \text{s}^{-1}$,
180 4.8-fold greater than the LTA value. This discrepancy is likely due to the shorter length
181 between LED and sample and small probe size. Because LED emission is conical (**Fig.**
182 **1c**), this length difference concentrates photons on the probe, artificially elevating

183 measured intensity values. This discrepancy could be eliminated using improved probe
184 designs.

185 Next, we benchmarked the effect of red light by outfitting the top and bottom
186 positions with 533 and 678 nm (red) LEDs and re-measured the green light response in
187 the presence of 2.00 – 12.00 $\mu\text{mol m}^{-2} \text{s}^{-1}$ red photons. We observed that dynamic range
188 and n_H remain unchanged while $k_{1/2}$ increases by 0.11 $\mu\text{mol m}^{-2} \text{s}^{-1}$ per 1.00 $\mu\text{mol m}^{-2} \text{s}^{-1}$
189 red light (**Fig. 3b** and **Supplementary Table 9**), consistent with our previous data.

190 Finally, we used the LPA to characterize the kinetic response of CcaS-CcaR to
191 step changes in green intensity. We observed a 4.5 min delay, an 11 min transcription
192 rate switching time, and sfGFP switching dynamics set by the cell division time (**Fig. 3c**),
193 equivalent to LTA results. We used these data to re-calibrate the parameters of our model
194 to the LPA conditions (**Methods** and **Supplementary Table 10**). Finally, we successfully
195 used the model to program sfGFP expression to follow a challenging waveform
196 comprising linear ramps, a hold, and a sine wave with high predictability (**Fig. 3d**). We
197 conclude that the LPA meets the same performance standards at the LTA.

198 Characterizing CcaS-CcaR forward and reverse action spectra.

199 The action spectrum is the relationship between input wavelength and output
200 activity. While all optogenetic tools have forward (ground state) action spectra (FAS),
201 photoreversible tools also have reverse (activated state) action spectra (RAS).

202 We next aimed to demonstrate that the LPA can be used to characterize the FAS
203 and RAS of optogenetic tools using CcaS-CcaR as a model. To this end, we outfitting the
204 bottom position of a device with LEDs of output wavelength between 364 and 947 nm
205 (**Fig. 1d** and **Supplementary Table 5**) and programmed each to emit 0.40 $\mu\text{mol m}^{-2} \text{s}^{-1}$,

206 or $2^*k_{1/2}$ for the 533 nm LED (**Fig. 3b**). We then measured the steady state response of
207 CcaS-CcaR to each input as before. This experiment reveals a maximal activating
208 wavelength of 533 nm and >50% maximal activation between 533 and 571 nm (**Fig. 4**).
209 We previously generated a course-grained map of the CcaS-CcaR FAS using six
210 wavelengths with a rudimentary instrument in an experiment that required approximately
211 one week⁸. By contrast, the LPA enables us to measure a 24 wavelength FAS in a single
212 day.

213 To characterize the RAS, we outfitted the top positions of a device with the 533 nm
214 LED and the bottom positions with the same LEDs used in the FAS experiment. We set
215 the 533 nm LED to $0.40 \mu\text{mol m}^{-2} \text{s}^{-1}$ and each bottom LED to $3.21 \mu\text{mol m}^{-2} \text{s}^{-1}$ because
216 CcaS-CcaR has approximately 10-fold greater sensitivity to green than red light (**Fig. 3b**).
217 Consistent with *in vitro* absorbance measurements of activated CcaS⁵³, exposure of our
218 CcaS-CcaR expressing strain to these inputs reveals maximal deactivation by the 678
219 nm LED (**Fig. 4**). To our knowledge, this is the first measurement of the RAS of an
220 optogenetic tool.

221 Characterizing the *S. cerevisiae* CRY2-CIB1 yeast two hybrid system.

222 Tucker and coworkers previously engineered a blue light activated *S. cerevisiae*
223 promoter system by fusing Cryptochrome 2 (CRY2) to the Gal4 DNA binding domain
224 (DBD) and the interaction domain of its blue-light dependent heterodimerizing partner
225 CIB1 to the Gal4 activation domain in a yeast two-hybrid (Y2H) system¹³ (**Fig. 5a**).

226 To demonstrate compatibility of the LPA with yeast, we characterized the CRY2-
227 CIB1 Y2H I/O. We outfitted the top and bottom positions of an LPA with 467 nm (blue)
228 LEDs, and programmed them to emit intensities between 0.26 and $1057.00 \mu\text{mol m}^{-2} \text{s}^{-1}$.

229 We grew yeast expressing CRY2-CIB1 Y2H with an mCherry output in a shaking LPA
230 under these conditions for 18 or 24 h and measured output using flow cytometry
231 (**Methods**). Between 0.26 and 93.50 $\mu\text{mol m}^{-2} \text{s}^{-1}$, mCherry increases in a Hill-like manner
232 with 5.6-fold dynamic range, n_H of 1.3 and $k_{1/2}$ of 10.74 $\mu\text{mol m}^{-2} \text{s}^{-1}$ (**Fig. 5b**), consistent
233 with previous reports^{13,26,54}. Though mCherry increases slightly at higher intensities, we
234 observe growth defects, likely due to heating or phototoxicity (**Supplementary Fig. 22**).

235 To characterize CRY2-CIB1 Y2H dynamics, we performed a step increase and
236 decrease in blue light and measured the mCherry response over time (**Methods**). We
237 observe a delay followed by an exponential increase (step-on) or decrease (step-off) in
238 mCherry to a final steady state (**Fig. 5c**). By fitting the data to a first order ODE model
239 with a delay (**Methods**), we quantify the delay to be 75.13 min, and the time to reach 50%
240 of the final mCherry level to be 222 min (**Supplementary Table 11**). The slower dynamics
241 compared to CcaS-CcaR are likely due to slower rates of transcriptional activation and
242 cell division, as well as the additional steps of mRNA processing and nuclear/cytoplasmic
243 transport.

244 Next, we measured the CRY2/CIB1 Y2H FAS by outfitting the bottom position of
245 an LPA with LEDs between 382 and 849 nm and programming their outputs to 88.80
246 $\mu\text{mol m}^{-2} \text{s}^{-1}$, the highest intensity possible without reducing the output of the dimmest
247 (533 nm) LED. This experiment reveals peak activation in response to the 382 nm and
248 467 nm LEDs and broad wavelength responsivity in the blue (>50% response from 382
249 to 503 nm) which matches the broad, multi-peaked in-vitro absorbance spectrum of
250 CRY2⁵⁵ (**Fig. 5d**). We conclude that the LPA is compatible with yeast optogenetic tools.

251

252 Spatial control of mammalian cell gene expression with PHYB/VNP-PIF6.

253 We recently modified the surface of viral nanoparticles (VNPs) with Phytochrome
254 Interacting Factor 6 (VNP-PIF6) to bind a heterologously expressed nuclear localization
255 sequence tagged Phytochrome B (PHYB-NLS) and deliver a transgene to the mammalian
256 cell nucleus in a red light activated, far-red deactivated manner⁵⁶ (**Fig. 6a**). Using an early
257 LPA prototype, we tuned delivery of *gfp* to HeLa cells from 35 to 600% that of wild-type
258 virus. Using custom photomasks, we also patterned GFP expression within different
259 regions of a confluent culture well. Delivery of red light alone resulted in low contrast
260 between cells inside and outside the pattern. Co-delivering far red reduced expression in
261 unwanted areas and increased contrast. However, this prototype had numerous
262 shortcomings including a requirement for a glass bottom plate that often fractured during
263 experiments.

264 To validate compatibility with mammalian cells and extend our previous results, we
265 outfitted the top and bottom positions of an LPA with 647 (red) and 735 nm (far red) LEDs
266 and replaced the plate adapter gasket (**Supplementary Fig. 17a**) with a laser-cut black
267 nitrile photomask (**Supplementary Fig. 17b**). We preconditioned HeLa cells in 6 wells of
268 1 plate with $2.00 \mu\text{mol m}^{-2} \text{s}^{-1}$ far red light for 30 min and then reduced it to $1.00 \mu\text{mol m}^{-2}$
269 s^{-1} while introducing variable red light between 0.25 and $4 \mu\text{mol m}^{-2} \text{s}^{-1}$ for 1 h. We
270 allowed GFP to accumulate during a 48 h dark incubation and then imaged the resulting
271 expression patterns by fluorescence microscopy (**Methods**). As expected, GFP
272 expression increases with red intensity (**Fig. 6b**). Additionally, the contrast ratio (GFP
273 intensity in exposed divided by that in non-exposed regions) reaches an optimal value of

274 16.6, near the maximum dynamic range of the system, at an intermediate red:far red ratio
275 of 2.5 (**Fig. 6c**).

276

277 Using the LPA to entrain the cyanobacterial circadian clock.

278 The cyanobacterium *Synechococcus elongatus* PCC7942 is a model for studying
279 circadian rhythm⁵⁷. Exposing cells to 12 h dark/12 h light cycles entrains the circadian
280 clock. After entrainment, a roughly 24 h transcriptional oscillation^{58,59} is maintained for
281 roughly 30-64% of the genome, even under constant light⁶⁰.

282 The time-intensive nature of the entrainment protocol makes it difficult to conduct
283 multiple parallel experiments in order to study clock properties and one group has recently
284 sought to simplify the procedure by using a computer-controlled LED array⁵¹. To examine
285 whether the LPA can be used to automate circadian entrainment, we outfitted the top and
286 bottom positions of three devices with 647 and 467 nm LEDs to provide a balanced
287 photosynthetic active radiation spectrum typical of grow lights. We programmed 6
288 different signals across the devices wherein cells were exposed to 3 cycles starting at
289 different times. Luminescence from a commonly used reporter system^{60,61} wherein
290 luciferase substrate is produced from the “dusk-peaking” promoter *psbAI* and luciferase
291 from the “dawn-peaking” promoter *kaiBC* was then measured (**Fig. 7a**). As expected, the
292 oscillations of cultures that were entrained starting at different times showed different
293 phases (**Fig. 7b**). The order of peaks in luminescence was also as expected, with the
294 cultures entrained starting at 0 h (red) peaking before cultures entrained starting at 4 h
295 (orange), 8 h (yellow), 12 h (green), 16 h (blue) and 20 h (purple) (**Fig. 7b,c**). However,

296 the position of the peaks exhibits some dispersion, potentially due to heating of the LPA
297 or the transition of cultures from the LPA to the plate reader.

298

299 **Discussion**

300 The LPA establishes new standards of flexibility, user-friendliness, and
301 affordability in non-neural optogenetics and photobiology hardware – features that should
302 facilitate widespread adoption. In terms of flexibility, the LPA is compatible with bacteria,
303 yeast, and mammalian cells and other common model organisms. The ~1 mL well volume
304 and the shaker adapters make the device compatible with most model organism growth
305 protocols. The diversity of available LEDs theoretically makes the LPA compatible with
306 all known genetically encoded photoreceptors and most photobiological processes. The
307 second LED position allows improved spatial and dynamical control of photoreversible
308 optogenetic tools and characterization of reverse action spectra. Different spatial patterns
309 can easily be applied by using laser cut gaskets. In addition to these features, the LPA
310 retains the high standards of programmability and experimental precision of the LTA⁴⁷.

311 The ease of assembly, intuitive Iris interface, simplified liquid handling, and
312 automated calibration script make the LPA user friendly. The LPA can be assembled
313 easily and quickly by a non-expert using fully documented assembly instructions and
314 tutorial videos. Iris converts high-level light function specifications into low level hardware
315 operations, greatly reducing programming requirements. LPA samples can be loaded and
316 harvested using a multichannel pipettor, and the plate can be sealed and unsealed with
317 an adhesive lid in a single step, facilitating high throughput experimentation. The plate is
318 also compatible with plate readers and plate-based flow cytometers, enabling direct

319 measurements of absorbance, fluorescence, or luminescence without additional liquid
320 handling. Finally, our MATLAB script simplifies calibration for experiments where the
321 same LED is used in multiple wells.

322 The LPA is more economical than comparable devices. The 24-well plate costs
323 \$7.70 and can be reused dozens of times, lowering per sample cost to <\$0.01.
324 Furthermore, the \$400 component cost drops to \$150 with access to a 3D printer. These
325 low costs make the LPA practical for large scale experiments (**Supplementary Fig. 23**).

326 The action spectra of optogenetic tools are seldom measured due to the lack of
327 convenient hardware. Using the LPA, both the FAS and RAS can be measured with 24
328 wavelength resolution in one experiment. This feature should permit improved
329 characterization of light responsive signaling pathways and enable cross-talk to be
330 minimized when using multiple optogenetic photoreceptors.

331 Despite early efforts^{62,63}, there is little data directly comparing the performance
332 features of optogenetic tools. Accordingly, researchers may have difficulty selecting the
333 best tool for a given experiment. On the other hand, the LPA can be used to directly
334 compare optogenetic tools, including those in different organisms. For example, in this
335 study we found that CRY2/CIB1 Y2H is 50 times less sensitive to light than CcaS-CcaR
336 (compare $k_{1/2}$ in **Figs. 3b, 5b**). Using the basic protocols established here, the LPA could
337 be used to quantitatively compare the spectral, intensity dependent, and dynamical
338 properties of all published optogenetic tools with gene expression outputs in bacteria,
339 yeast, mammalian cells and other organisms, providing much needed information to the
340 community that should accelerate the adoption of optogenetics.

341 Many circadian assays, such as those measuring the sensitivity of the rhythm to
342 optical perturbations as a function of time of day, are onerous and present a significant
343 barrier to the researcher. The LPA provides a compact and economical solution to this
344 problem. Additionally, the ability to program two wavelengths may ease studies of
345 organisms and processes that respond differently to different wavelengths such as phase
346 resetting in the green algae *C. reinhardtii* in which shifts in the circadian rhythm are
347 wavelength dependent as a function of cellular status. The ability to program 24 light
348 signals simultaneously may also ease experiments such as testing growth of mutants with
349 longer or shorter circadian periods with different lengths of light and dark^{64–66}.

350 By releasing the LPA and Iris with an open-source license, we aim to incorporate
351 other researchers as developers to extend and improve the platform. Similar to a recent
352 example⁶⁷ we have made all design files, a bill of materials, and protocols needed to
353 fabricate, assemble, and operate the device, as well as standard format source code on
354 a public version control system freely available. From this repository, the community can
355 download up-to-date file versions, suggest or make improvements or modifications,
356 design new accessories, and upload all updates for others to use and build upon further.
357 Future designs could incorporate more LEDs per well, sample injection, and on-board
358 sensors for measurement of absorbance, fluorescence, or luminescence, enabling
359 optogenetic feedback control⁶⁸. Better heat dissipation for high intensity experiments
360 could be achieved through addition of heat sinks, fans, chassis parts with better
361 ventilation, or even active temperature feedback control. 96-well or greater plate format
362 designs should also be possible. With 3D printing and microcontroller technologies
363 becoming increasingly inexpensive and accessible, such advances can be made by

364 researchers without formal electrical and mechanical engineering backgrounds. We hope
365 that this work not only enables new researchers to perform optogenetics and photobiology
366 experiments, but also motivates them join the growing open-hardware community.

367

368 **Methods**

369 *LPA*

370 Detailed descriptions of LPA design, fabrication, assembly, calibration, and operation,
371 and CAD files and firmware are included in **Supplementary Information**. The most up-
372 to-date documentation and file versions can be found at taborlab.rice.edu/hardware.

373

374 *Iris*

375 Source code and detailed descriptions of the staggered start algorithm, waveform
376 handling, file specifications, randomization and de-randomization procedure, and LPF
377 creation using Python are included in **Supplementary Information**. The most up-to-date
378 documentation and source code can be accessed at taborlab.rice.edu/software.

379

380 *CcaS-CcaR*

381 To make frozen starter aliquots, a 3 mL LB + 50 µg/mL kanamycin, 100 µg/mL
382 spectinomycin and 34 µg/mL chloramphenicol culture was inoculated from a -80°C stock
383 and grown (37°C, 250 rpm) to $OD_{600} < 0.3$. 30% glycerol was added, absorbance
384 measured, and 50µL aliquots made and stored at -80°C. For experiments, M9 +
385 antibiotics was inoculated with a starter aliquot, to $OD_{600} = 0.00015$. 500 µL starter culture
386 was added to each well of the 24-well plate and the plate was sealed with adhesive foil.

387 The plate was placed into the LPA and the assembly mounted on a shaker/incubator at
388 37°C, 250 rpm for 8 h. The plate was then removed and chilled in an ice-water bath. Cells
389 were chilled for ≥ 15 min and the foil removed. 200 μ L from each well was transferred to
390 flow cytometry tubes containing 1 mL PBS, and cells were treated with rifampicin as
391 before⁴⁷.

392

393 *CRY2-CIB1 Y2H*

394 A 3 mL SD (-Ura, -Trp, -Leu) medium starter culture was inoculated from a -80°C stock
395 and grown (30°C, 250 r.p.m) overnight to a final density of approximately $OD_{600} = 2$. The
396 starter culture was diluted into fresh SD to $OD_{600} = 0.001$. The plate was prepared and
397 loaded/unloaded as with *E. coli*. Cells were grown in the LPA (30°C, 250 rpm) for 24 h
398 (step-off dynamics experiments) or 18 h (other experiments). Samples were harvested as
399 described for *E. coli* without rifampicin treatment.

400

401 *Flow cytometry*

402 Cytometry was performed with a BD FACScan flow cytometer as previously⁴⁷. Settings
403 used for each experiment are listed in **Supplementary Table 12**. Typical count rates of
404 1,000–2,000 events/s were used and approximately 20,000 events were captured for
405 each sample. Calibration beads (RCP-30-5A, Spherotech) were measured at each
406 session. Data was processed and sfGFP and mCherry fluorescence were calibrated to
407 Molecules of Equivalent Fluorescein (MEFL) and Molecules of Equivalent Cy5 (MECY)
408 with FlowCal⁶⁹.

409

410 *CcaS-CcaR model*

411 Data was modeled as previously⁴⁷. Parameter fitting was performed in GraphPad. All
412 parameters were constrained to > 0 , and τ_{delay} and k_g are shared between step-on and
413 step-off data sets.

414

415 *CRY2-CIB1 Y2H model*

416 We apply a first order linear ODE model

417
$$\frac{dm}{dt} = \alpha(c(I_b, t') - m(t))$$

418

419
$$m(t < \tau_{delay}) = m_0 = c(I_b, t < \tau_{delay}) = c_{precondition}$$

420

421 where the rate of change of mCherry, $m(t)$, is a function of the difference between
422 the mCherry “set-point”, $c(t')$ and the current mCherry concentration. $c(t')$ is blue light
423 intensity, I_b , mapped to mCherry units through the steady-state transfer function at when
424 the light signal last changed, $t' = t - \tau_{delay}$. At $t < \tau_{delay}$, mCherry is equal to its initial
425 value, which is determined by the preconditioning set-point, $c_{precondition}$.

426 The solution to this ODE has the following piece-wise form:

427

428
$$m(t') = \begin{cases} m_0 & , \quad t' \leq 0 \\ c + (m_0 - c)e^{-\alpha t'} & , \quad t' \geq 0 \end{cases}$$

429

430 where mCherry remains at its initial value, m_0 , for $t \leq \tau_{delay}$, and exponentially
431 increases or decreases with rate constant α for $t \geq \tau_{delay}$.

432 Parameter fitting was performed by nonlinear least squares in GraphPad. All
433 parameters were constrained to > 0 , and τ_{delay} and α were shared between step-on and
434 step-off data sets.

435

436 *PHYB/VNP-PIF6*

437 Experimental protocols were as described⁵⁶ except that three sheets of diffuser paper
438 (#3008, Rosco) were used in place of the LED spacer gasket. Adhesive foil was not used
439 to avoid interference from reflected light.

440

441 *Synechococcus Native Circadian Rhythm*

442 1.5ml of a culture of AMC462⁷⁰ growing in exponential phase diluted to OD₇₅₀ 0.05
443 was pipetted into each well of the 24-well cell culture plate. Extra distilled water was
444 pipetted between wells to reduce evaporation, and the plate was covered with a
445 transparent lid (Visiplate 24-TC Part: 1450-6045) with adhesive foil (F96VWR100). The
446 cells were then grown at 30° C with shaking at 255 rpm for 4 days.

447

448 *Luminescence data acquisition and analysis*

449 Luminescence of 150 μ l of culture in a 96-well black with clear bottom plate with
450 transparent lid was measured using a Tecan M200 with a luminescence module and an
451 integration time of 1000 ms. Between readings, the plate was moved out of the machine
452 for 20 min and kept under a fluorescent lamp at 4500 lux. Readings were taken for a total
453 of 160 h.

454 Luminesce data was fitted with BRASS (Biological Rhythms Analysis Software
455 System; A. J. Millar laboratory, University of Edinburgh, Scotland, United Kingdom) and
456 FFT-NLLS (Fast Fourier Transform-Nonlinear Least Squares)^{71,72}. At least 72 h of each
457 culture was included in the analysis.

458 The best fits for the expected phases were calculated by minimizing the root mean
459 square distance from the location of the expected phase to the location of experimental
460 phase using the GRG Nonlinear solving method in Excel.

461

462 **References:**

- 463 1. Boyden, E. S., Zhang, F., Bamberg, E., Nagel, G. & Deisseroth, K. Millisecond-
464 timescale, genetically targeted optical control of neural activity. *Nat. Neurosci.* **8**,
465 1263–8 (2005).
- 466 2. Deisseroth, K. Optogenetics: 10 years of microbial opsins in neuroscience. *Nat.*
467 *Neurosci.* **18**, 1213–1225 (2015).
- 468 3. Aravanis, A. M. *et al.* An optical neural interface: in vivo control of rodent motor
469 cortex with integrated fiberoptic and optogenetic technology. *J. Neural Eng.* **4**,
470 S143–56 (2007).
- 471 4. Adamantidis, A. R., Zhang, F., Aravanis, A. M., Deisseroth, K. & de Lecea, L.
472 Neural substrates of awakening probed with optogenetic control of hypocretin
473 neurons. *Nature* **450**, 420–4 (2007).
- 474 5. Shimizu-Sato, S., Huq, E., Tepperman, J. M. & Quail, P. H. A light-switchable
475 gene promoter system. *Nat. Biotechnol.* **20**, 1041–4 (2002).

- 476 6. Levskaya, A. *et al.* Synthetic biology: engineering Escherichia coli to see light.
477 *Nature* **438**, 441–2 (2005).
- 478 7. Möglich, A., Ayers, R. A. & Moffat, K. Design and signaling mechanism of light-
479 regulated histidine kinases. *J. Mol. Biol.* **385**, 1433–44 (2009).
- 480 8. Tabor, J. J., Levskaya, A. & Voigt, C. A. Multichromatic control of gene expression
481 in Escherichia coli. *J. Mol. Biol.* **405**, 315–24 (2011).
- 482 9. Ohlendorf, R., Vidavski, R. R., Eldar, A., Moffat, K. & Möglich, A. From dusk till
483 dawn: one-plasmid systems for light-regulated gene expression. *J. Mol. Biol.* **416**,
484 534–42 (2012).
- 485 10. Schmidl, S. R., Sheth, R. U., Wu, A. & Tabor, J. J. Refactoring and optimization of
486 light-switchable Escherichia coli two-component systems. *ACS Synth. Biol.* **3**,
487 820–31 (2014).
- 488 11. Ryu, M.-H. & Gomelsky, M. Near-infrared light responsive synthetic c-di-GMP
489 module for optogenetic applications. *ACS Synth. Biol.* **3**, 802–10 (2014).
- 490 12. Abe, K. *et al.* Engineering of a green-light inducible gene expression system in
491 Synechocystis sp. PCC6803. *Microb. Biotechnol.* **7**, 177–83 (2014).
- 492 13. Kennedy, M. J. *et al.* Rapid blue-light-mediated induction of protein interactions in
493 living cells. *Nat. Methods* **7**, 973–5 (2010).
- 494 14. Rizzini, L. *et al.* Perception of UV-B by the Arabidopsis UVR8 protein. *Science*
495 **332**, 103–6 (2011).
- 496 15. Ye, H., Daoud-El Baba, M., Peng, R.-W. & Fussenegger, M. A synthetic
497 optogenetic transcription device enhances blood-glucose homeostasis in mice.

- 498 *Science* **332**, 1565–8 (2011).
- 499 16. Polstein, L. R. & Gersbach, C. A. Light-inducible spatiotemporal control of gene
500 activation by customizable zinc finger transcription factors. *J. Am. Chem. Soc.*
501 **134**, 16480–3 (2012).
- 502 17. Wang, X., Chen, X. & Yang, Y. Spatiotemporal control of gene expression by a
503 light-switchable transgene system. *Nat. Methods* **9**, 266–9 (2012).
- 504 18. Crefcoeur, R. P., Yin, R., Ulm, R. & Halazonetis, T. D. Ultraviolet-B-mediated
505 induction of protein-protein interactions in mammalian cells. *Nat. Commun.* **4**,
506 1779 (2013).
- 507 19. Konermann, S. *et al.* Optical control of mammalian endogenous transcription and
508 epigenetic states. *Nature* **500**, 472–6 (2013).
- 509 20. Müller, K. *et al.* A red/far-red light-responsive bi-stable toggle switch to control
510 gene expression in mammalian cells. *Nucleic Acids Res.* **41**, e77 (2013).
- 511 21. Motta-Mena, L. B. *et al.* An optogenetic gene expression system with rapid
512 activation and deactivation kinetics. *Nat. Chem. Biol.* **10**, 196–202 (2014).
- 513 22. Müller, K., Engesser, R., Timmer, J., Zurbriggen, M. D. & Weber, W. Orthogonal
514 optogenetic triple-gene control in Mammalian cells. *ACS Synth. Biol.* **3**, 796–801
515 (2014).
- 516 23. Nihongaki, Y., Yamamoto, S., Kawano, F., Suzuki, H. & Sato, M. CRISPR-Cas9-
517 based photoactivatable transcription system. *Chem. Biol.* **22**, 169–74 (2015).
- 518 24. Polstein, L. R. & Gersbach, C. A. A light-inducible CRISPR-Cas9 system for
519 control of endogenous gene activation. *Nat. Chem. Biol.* **11**, 198–200 (2015).

- 520 25. Chan, Y.-B., Alekseyenko, O. V & Kravitz, E. A. Optogenetic Control of Gene
521 Expression in *Drosophila*. *PLoS One* **10**, e0138181 (2015).
- 522 26. Liu, H., Gomez, G., Lin, S., Lin, S. & Lin, C. Optogenetic control of transcription in
523 zebrafish. *PLoS One* **7**, e50738 (2012).
- 524 27. Müller, K. *et al.* A red light-controlled synthetic gene expression switch for plant
525 systems. *Mol. Biosyst.* **10**, 1679–88 (2014).
- 526 28. Cao, J. *et al.* Light-inducible activation of target mRNA translation in mammalian
527 cells. *Chem. Commun. (Camb)*. **49**, 8338–40 (2013).
- 528 29. Walsh, S., Gardner, L., Deiters, A. & Williams, G. J. Intracellular light-activation of
529 riboswitch activity. *Chembiochem* **15**, 1346–51 (2014).
- 530 30. Renicke, C., Schuster, D., Usherenko, S., Essen, L.-O. & Taxis, C. A LOV2
531 domain-based optogenetic tool to control protein degradation and cellular
532 function. *Chem. Biol.* **20**, 619–26 (2013).
- 533 31. Levskaya, A., Weiner, O. D., Lim, W. A. & Voigt, C. A. Spatiotemporal control of
534 cell signalling using a light-switchable protein interaction. *Nature* **461**, 997–1001
535 (2009).
- 536 32. Dueber, J. E. *et al.* Synthetic protein scaffolds provide modular control over
537 metabolic flux. *Nat. Biotechnol.* **27**, 753–9 (2009).
- 538 33. Gautier, A., Deiters, A. & Chin, J. W. Light-activated kinases enable temporal
539 dissection of signaling networks in living cells. *J. Am. Chem. Soc.* **133**, 2124–7
540 (2011).
- 541 34. Toettcher, J. E., Gong, D., Lim, W. A. & Weiner, O. D. Light-based feedback for

- 542 controlling intracellular signaling dynamics. *Nat. Methods* **8**, 837–9 (2011).
- 543 35. Ye, H., Daoud-El Baba, M., Peng, R.-W. & Fussenegger, M. A synthetic
544 optogenetic transcription device enhances blood-glucose homeostasis in mice.
545 *Science* **332**, 1565–8 (2011).
- 546 36. Bugaj, L. J., Choksi, A. T., Mesuda, C. K., Kane, R. S. & Schaffer, D. V.
547 Optogenetic protein clustering and signaling activation in mammalian cells. *Nat.*
548 *Methods* **10**, 249–52 (2013).
- 549 37. Toettcher, J. E., Weiner, O. D. & Lim, W. A. Using optogenetics to interrogate the
550 dynamic control of signal transmission by the Ras/Erk module. *Cell* **155**, 1422–34
551 (2013).
- 552 38. Wend, S. *et al.* Optogenetic control of protein kinase activity in mammalian cells.
553 *ACS Synth. Biol.* **3**, 280–5 (2014).
- 554 39. Bugaj, L. J. *et al.* Regulation of endogenous transmembrane receptors through
555 optogenetic Cry2 clustering. *Nat. Commun.* **6**, 6898 (2015).
- 556 40. Chen, D., Gibson, E. S. & Kennedy, M. J. A light-triggered protein secretion
557 system. *J. Cell Biol.* **201**, 631–40 (2013).
- 558 41. Niopek, D. *et al.* Engineering light-inducible nuclear localization signals for precise
559 spatiotemporal control of protein dynamics in living cells. *Nat. Commun.* **5**, 4404
560 (2014).
- 561 42. Beyer, H. M. *et al.* Red Light-Regulated Reversible Nuclear Localization of
562 Proteins in Mammalian Cells and Zebrafish. *ACS Synth. Biol.* **4**, 951–8 (2015).
- 563 43. Yumerefendi, H. *et al.* Control of Protein Activity and Cell Fate Specification via

- 564 Light-Mediated Nuclear Translocation. *PLoS One* **10**, e0128443 (2015).
- 565 44. Niopek, D., Wehler, P., Roensch, J., Eils, R. & Di Ventura, B. Optogenetic control
566 of nuclear protein export. *Nat. Commun.* **7**, 10624 (2016).
- 567 45. Nihongaki, Y., Kawano, F., Nakajima, T. & Sato, M. Photoactivatable CRISPR-
568 Cas9 for optogenetic genome editing. *Nat. Biotechnol.* **33**, 755–760 (2015).
- 569 46. Hemphill, J., Borchardt, E. K., Brown, K., Asokan, A. & Deiters, A. Optical Control
570 of CRISPR/Cas9 Gene Editing. *J. Am. Chem. Soc.* **137**, 5642–5 (2015).
- 571 47. Olson, E. J., Hartsough, L. A., Landry, B. P., Shroff, R. & Tabor, J. J.
572 Characterizing bacterial gene circuit dynamics with optically programmed gene
573 expression signals. *Nat. Methods* **11**, 449–55 (2014).
- 574 48. Richter, F. *et al.* Upgrading a microplate reader for photobiology and all-optical
575 experiments. *Photochem. Photobiol. Sci.* **14**, 270–9 (2015).
- 576 49. Davidson, E. A., Basu, A. S. & Bayer, T. S. Programming microbes using pulse
577 width modulation of optical signals. *J. Mol. Biol.* **425**, 4161–6 (2013).
- 578 50. Lee, J. M., Lee, J., Kim, T. & Lee, S. K. Switchable gene expression in
579 *Escherichia coli* using a miniaturized photobioreactor. *PLoS One* **8**, e52382
580 (2013).
- 581 51. Pattanayak, G. K., Phong, C. & Rust, M. J. Rhythms in energy storage control the
582 ability of the cyanobacterial circadian clock to reset. *Curr. Biol.* **24**, 1934–8 (2014).
- 583 52. Müller, K., Zurbriggen, M. D. & Weber, W. Control of gene expression using a red-
584 and far-red light-responsive bi-stable toggle switch. *Nat. Protoc.* **9**, 622–32 (2014).
- 585 53. Hirose, Y., Shimada, T., Narikawa, R., Katayama, M. & Ikeuchi, M.

- 586 Cyanobacteriochrome CcaS is the green light receptor that induces the
587 expression of phycobilisome linker protein. *Proc. Natl. Acad. Sci. U. S. A.* **105**,
588 9528–33 (2008).
- 589 54. Melendez, J. *et al.* Real-time optogenetic control of intracellular protein
590 concentration in microbial cell cultures. *Integr. Biol. (Camb)*. **6**, 366–72 (2014).
- 591 55. Li, X. *et al.* Arabidopsis cryptochrome 2 (CRY2) functions by the photoactivation
592 mechanism distinct from the tryptophan (trp) triad-dependent photoreduction.
593 *Proc. Natl. Acad. Sci. U. S. A.* **108**, 20844–9 (2011).
- 594 56. Gomez, E. J., Gerhardt, K., Judd, J., Tabor, J. J. & Suh, J. Light-Activated
595 Nuclear Translocation of Adeno-Associated Virus Nanoparticles Using
596 Phytochrome B for Enhanced, Tunable, and Spatially Programmable Gene
597 Delivery. *ACS Nano* acsnano.5b05558 (2015). doi:10.1021/acsnano.5b05558
- 598 57. Golden, S. S., Ishiura, M., Johnson, C. H. & Kondo, T. CYANOBACTERIAL
599 CIRCADIAN RHYTHMS. *Annu. Rev. Plant Physiol. Plant Mol. Biol.* **48**, 327–354
600 (1997).
- 601 58. Ito, H. *et al.* Cyanobacterial daily life with Kai-based circadian and diurnal
602 genome-wide transcriptional control in *Synechococcus elongatus*. *Proc. Natl.*
603 *Acad. Sci. U. S. A.* **106**, 14168–73 (2009).
- 604 59. Vijayan, V., Zuzow, R. & O’Shea, E. K. Oscillations in supercoiling drive circadian
605 gene expression in cyanobacteria. *Proc. Natl. Acad. Sci. U. S. A.* **106**, 22564–8
606 (2009).
- 607 60. Kondo, T. *et al.* Circadian rhythms in prokaryotes: luciferase as a reporter of

- 608 circadian gene expression in cyanobacteria. *Proc. Natl. Acad. Sci. U. S. A.* **90**,
609 5672–6 (1993).
- 610 61. Katayama, M., Tsinoremas, N. F., Kondo, T. & Golden, S. S. *cpmA*, a gene
611 involved in an output pathway of the cyanobacterial circadian system. *J. Bacteriol.*
612 **181**, 3516–24 (1999).
- 613 62. Gautier, A. *et al.* How to control proteins with light in living systems. *Nat. Chem.*
614 *Biol.* **10**, 533–41 (2014).
- 615 63. Pathak, G. P., Strickland, D., Vrana, J. D. & Tucker, C. L. Benchmarking of optical
616 dimerizer systems. *ACS Synth. Biol.* **3**, 832–8 (2014).
- 617 64. Johnson, C. H., Kondo, T. & Hastings, J. W. Action Spectrum for Resetting the
618 Circadian Phototaxis Rhythm in the CW15 Strain of *Chlamydomonas*: II.
619 Illuminated Cells. *Plant Physiol.* **97**, 1122–9 (1991).
- 620 65. Kondo, T., Johnson, C. H. & Hastings, J. W. Action Spectrum for Resetting the
621 Circadian Phototaxis Rhythm in the CW15 Strain of *Chlamydomonas*: I. Cells in
622 Darkness. *Plant Physiol.* **95**, 197–205 (1991).
- 623 66. Ma, P., Woelfle, M. A. & Johnson, C. H. An Evolutionary Fitness Enhancement
624 Conferred by the Circadian System in Cyanobacteria. *Chaos. Solitons. Fractals*
625 **50**, 65–74 (2013).
- 626 67. Takahashi, C. N., Miller, A. W., Ekness, F., Dunham, M. J. & Klavins, E. A low
627 cost, customizable turbidostat for use in synthetic circuit characterization. *ACS*
628 *Synth. Biol.* **4**, 32–8 (2015).
- 629 68. Miliias-Argeitis, A. *et al.* In silico feedback for in vivo regulation of a gene

- 630 expression circuit. *Nat. Biotechnol.* **29**, 1114–6 (2011).
- 631 69. Castillo-Hair, S. M. *et al.* FlowCal: A user-friendly, open source software tool for
632 automatically converting flow cytometry data from arbitrary to calibrated units.
633 *ACS Synth. Biol.* (2016). doi:10.1021/acssynbio.5b00284
- 634 70. Mackey, S. R., Ditty, J. L., Clerico, E. M. & Golden, S. S. Detection of rhythmic
635 bioluminescence from luciferase reporters in cyanobacteria. *Methods Mol. Biol.*
636 **362**, 115–29 (2007).
- 637 71. Plautz, J. D. *et al.* Quantitative analysis of *Drosophila* period gene transcription in
638 living animals. *J. Biol. Rhythms* **12**, 204–17 (1997).
- 639 72. Straume, M., Frasier-Cadoret, S. G. & Johnson, M. L. *Topics in Fluorescence*
640 *Spectroscopy*, **2**, (Kluwer Academic Publishers, 2002).

641

642 **Acknowledgements**

643 We thank M. McClean for providing yMM1146 and yMM1081, S. Golden for
644 *Synechococcus* AMC462, and M. Romer for assistance with *Synechococcus*
645 experiments. This work was supported by the ONR (MURI N000141310074), NSF (EFRI-
646 1137266), and NIH (1R21AI115014-01A1). B.L. is supported by an NDSEG Fellowship.
647 L.H. was supported by NASA NSTRF NNX11AN39H. E.J.G. is supported by a Ford
648 Foundation Fellowship. The cyanobacterial work was supported by a DOE Office of
649 Science Early Career Research Program (DE-SC0006394) to D.S. and R.Y. is a Simons
650 Foundation Fellow of the Life Sciences Research Foundation.

651

652 **Author Contributions**

653 K.G., E.O., and J.T. conceived of the project. K.G. (chassis and auxillary parts), E.O. and
654 S.C. (circuit board) designed the LPA. K.G, E.O., and P.R. built LPAs. S.C. designed and
655 wrote the LPA firmware and calibration software. L.H., B.L., and F.E. designed and wrote
656 Iris with equal contributions. K.G., E.O., and J.T. (*E. coli*, *S. cerevisiae* and mammalian)
657 and R.Y. and D.S. (cyanobacteria) designed experiments. K.G. (*E. coli*, *S. cerevisiae*),
658 E.G. (mammalian), and R.Y. (cyanobacteria) performed experiments, and K.G. and R.Y.
659 analyzed results. J.T., K.G., E.O., L.H., S.C., R.Y. and D.S. wrote the manuscript. J.S.,
660 D.S. and J.T. supervised the project.

661

662 **Competing Financial Interests**

663 The authors declare no competing financial interests.

664

665 **Materials and Correspondence**

666 Correspondence and material requests should be addressed to J.J.T
667 (jeff.tabor@rice.edu).

668

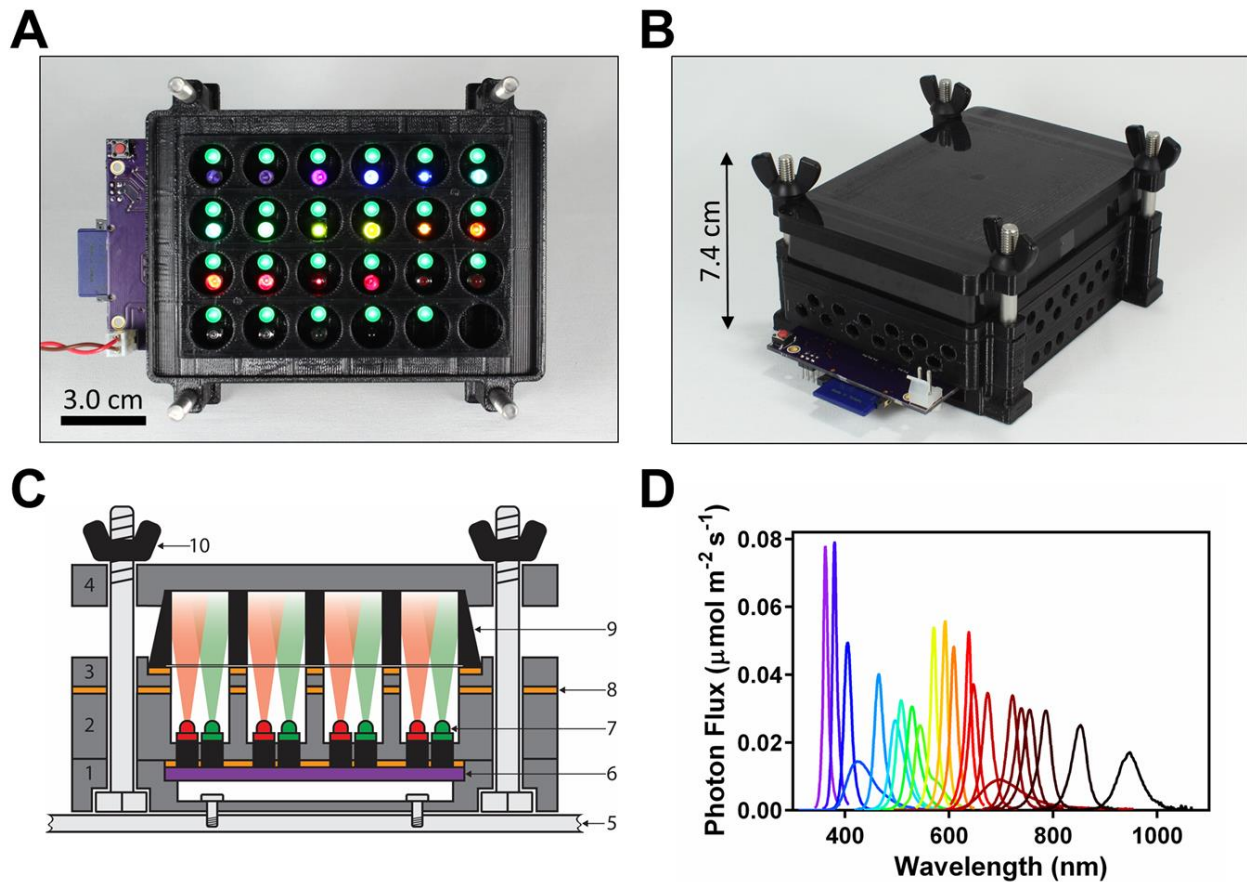
669 **Supplementary Information**

670 Documentation and procedures for the LPA and Iris, best-fit parameters, cytometry
671 settings, phototoxicity and/or LPA heating measurements are included in Supplementary
672 Information. CAD files, firmware, Iris source code, image analysis calibration script,
673 example calibration files, and supplementary videos are included in Supplementary Files.

674

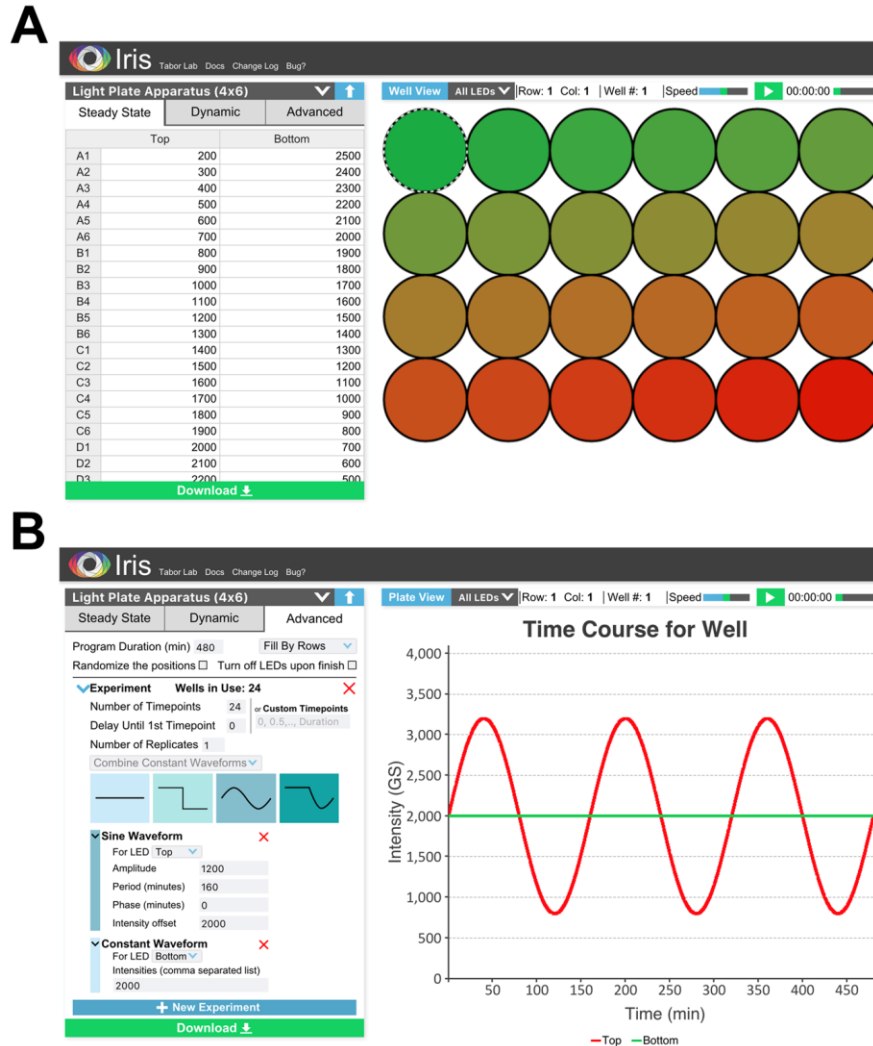
675

676 **Figures**



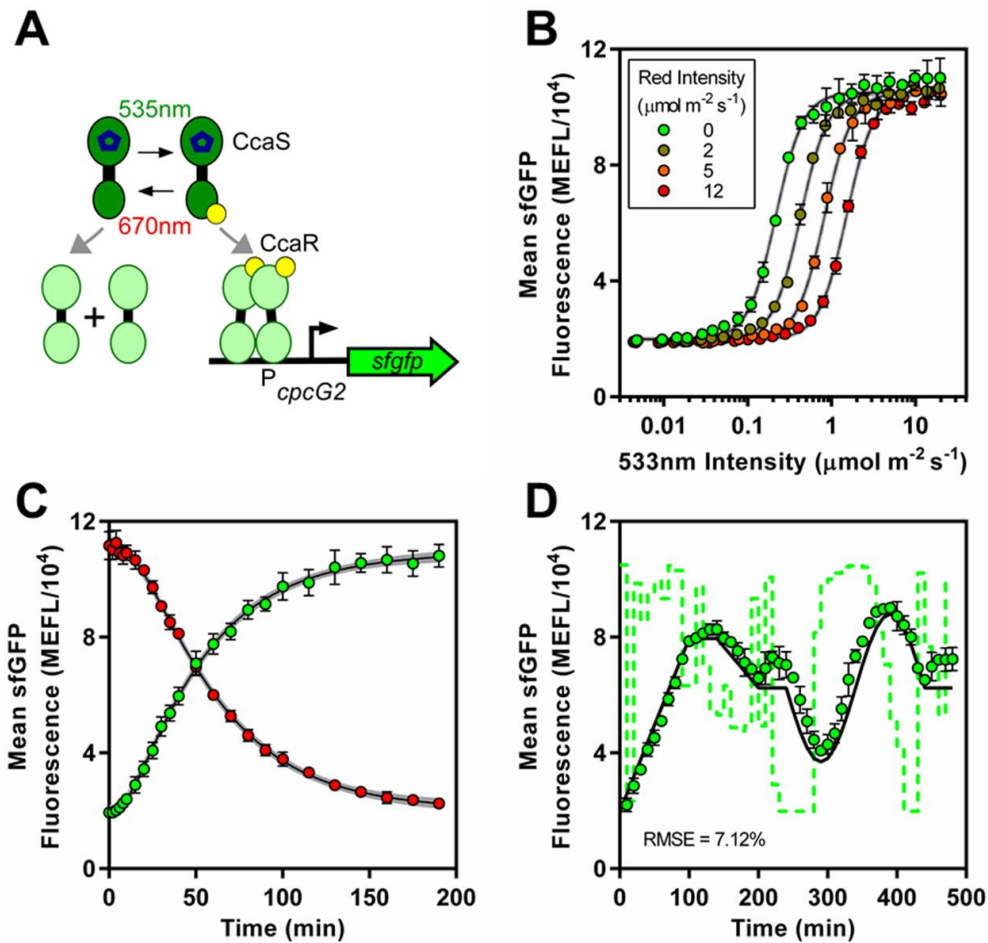
677

678 **Figure 1.** The LPA. **(a)** Top-down view of an LPA lacking the 24-well plate and plate lid.
679 In the configuration shown, the device contains a 535 nm LED in each top position and a
680 variable wavelength LED (364-947 nm) in each bottom position. The SD card (blue),
681 circuit board (purple), reset button (red) and power cord (red/black wires) are visible. **(b)**
682 Fully assembled LPA. **(c)** Schematic cross-section showing the light path from the LEDs
683 to the culture plate wells. (1) mounting plate, (2) LED spacer, (3) plate adapter, (4) plate
684 lid, (5) PCB, (6) LED atop LED socket, (7) gasket, (8) 24 well plate, (9) wing nut
685 assembled with mounting bolt. **(d)** Spectra of 22 LEDs (**Supplementary Table 5**) used in
686 this study measured and calibrated using a spectrophotometer and probe adapter
687 (**Supplementary Figs. 6b, 20, and Supplementary Procedure 8**).



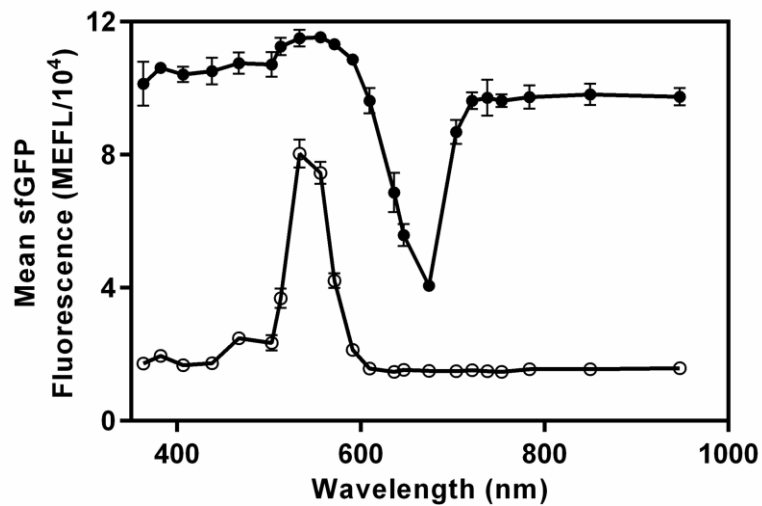
688

689 **Figure 2. Iris. (a) Steady State Mode.** Constant light functions are specified by entering
690 the desired greyscale intensity (0-4095) of up to all 48 LEDs in the Input Panel
691 spreadsheet (left). The download button is shown at the bottom of the Input Panel. In
692 Plate View mode (shown), the Simulation Panel (right) displays a schematic visualization
693 of the output intensity of all 48 LEDs. The top and bottom LEDs are visualized as red and
694 green, respectively, regardless of the actual LEDs used. **(b) Advanced Mode.** Constant
695 and dynamic light functions are specified in the Input Panel. In the latter case, Iris
696 automatically runs a staggered-start algorithm (**Supplementary Fig. 19**). In Well View
697 mode (shown), the Simulation Panel (right) visualizes the output of the top and bottom
698 LEDs in a given well over the duration of the experiment. The Simulation Panel also plays
699 movies of specified light function

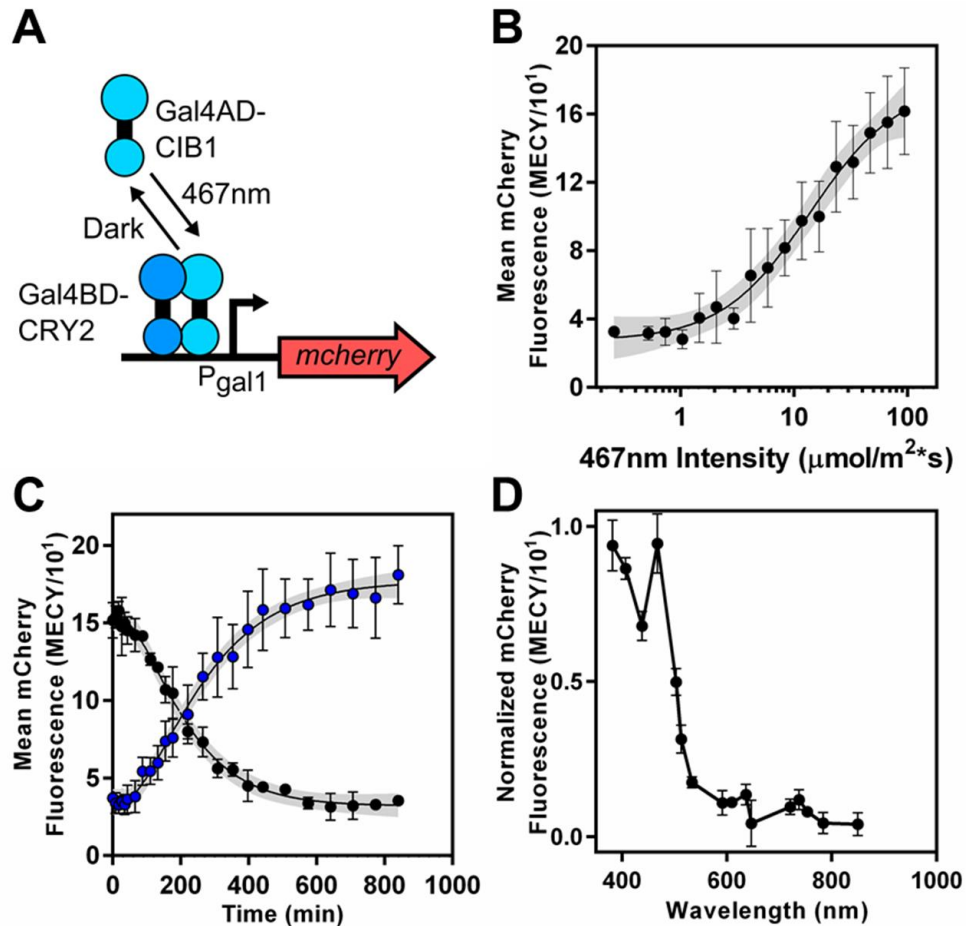


700

701 **Figure 3.** Benchmarking the LPA against *E. coli* CcaS-CcaR. **(a)** CcaS-CcaR system. **(b)**
702 CcaS-CcaR 533 nm light intensity versus sfGFP transfer functions in the presence of
703 increasing 678 nm. **(c)** Kinetic response to an increase in 533 nm light from 0.00 to 17.88
704 $\mu\text{mol m}^{-2} \text{s}^{-1}$ and simultaneous decrease in 678 nm light from 12.79 $\mu\text{mol m}^{-2} \text{s}^{-1}$ to 0.00
705 $\mu\text{mol m}^{-2} \text{s}^{-1}$ (green dots), or decrease in 533 nm light from 17.88 to 0.00 $\mu\text{mol m}^{-2} \text{s}^{-1}$ and
706 simultaneous increase in 678 nm from 0.00 $\mu\text{mol m}^{-2} \text{s}^{-1}$ to 12.79 $\mu\text{mol m}^{-2} \text{s}^{-1}$ (red dots).
707 Black lines represent best fits (**Supplementary Table 9** and **10**) of our previous CcaS-
708 CcaR mathematical model⁴⁷ to these data. Gray envelopes represent 95% confidence
709 intervals. **(d)** Biological Function Generation. Reference waveform (black line), pre-
710 computed 533 nm light intensity time course (green dashed lines), experimental sfGFP
711 levels (green dots). Constant 12.79 $\mu\text{mol m}^{-2} \text{s}^{-1}$ 678 nm was applied. 533 nm intensity
712 values are mapped to sfGFP units through the transfer function in panel a. RMSE
713 between experimental data and reference over three days is shown. Error bars represent
714 the SEM of three experiments over three days.

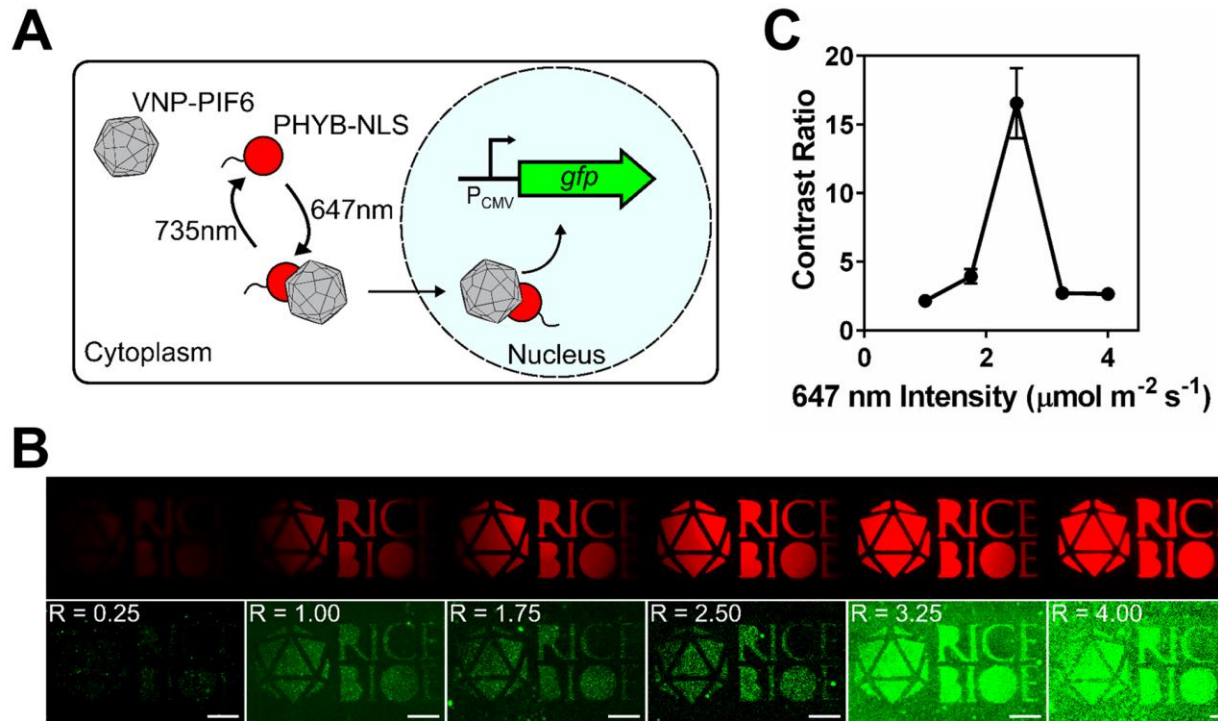


715
716 **Figure 4.** Using the LPA to characterize CcaS-CcaR forward and reverse action spectra.
717 For the FAS (hollow circles), bacteria were exposed to $0.397 \mu\text{mol m}^{-2} \text{s}^{-1}$ photons from a
718 variable wavelength bottom LED (**Fig. 1a,c**). For the RAS (black circles), bacteria were
719 exposed to $0.397 \mu\text{mol m}^{-2} \text{s}^{-1}$ from the maximally activating 533 nm LED in the top
720 position and $3.21 \mu\text{mol m}^{-2} \text{s}^{-1}$ photons from the variable wavelength bottom LED. Error
721 bars represent the SEM of three experiments over a single day.



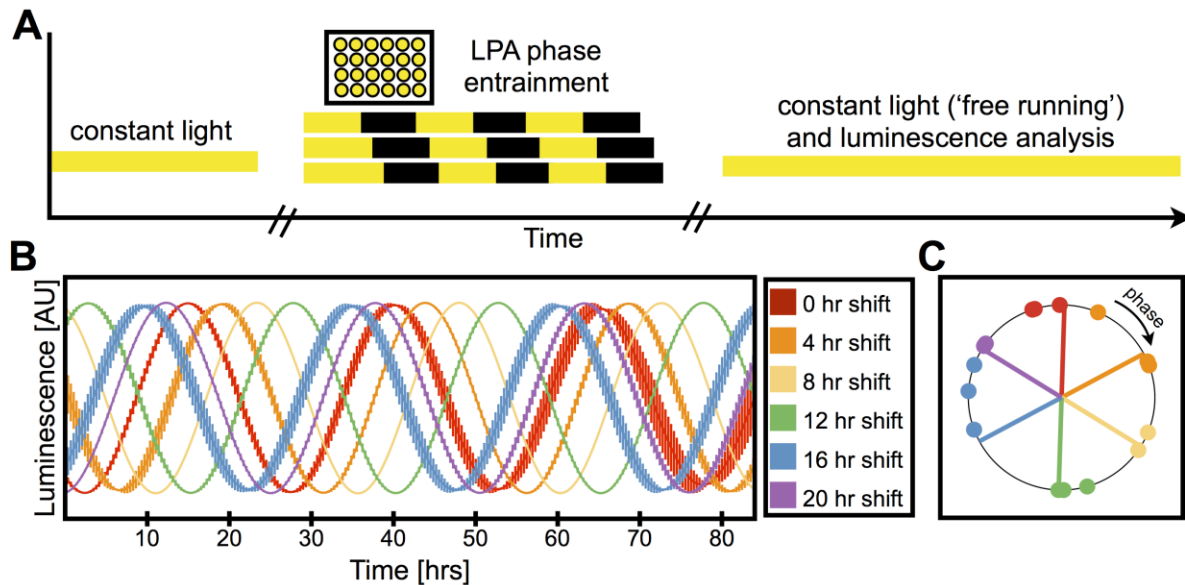
722
723
724
725
726
727
728
729
730
731
732

Figure 5. Validating the LPA with yeast by characterizing *S. cerevisiae* CRY2-CIB1 Y2H. **(a)** CRY2-CIB1 Y2H system. **(b)** 467 nm intensity transfer function. The black line represents the best fit to a Hill function. **(c)** Step activation and de-activation kinetics. Cells were either preconditioned for 4 h in the dark and switched to 88.8 μmol m⁻² s⁻¹ 467 nm (blue dots) or preconditioned in 88.8 μmol m⁻² s⁻¹ 467 nm for 10 h and switched to dark (black dots) at time zero. Black lines represent best fits (**Supplementary Tables 9** and **11**) to a kinetic model (**Methods**). **(d)** FAS. Experiments were performed as in **Figure 3a**, but with 88.8 μmol m⁻² s⁻¹ photon flux. Grey envelopes represent 95% confidence interval. Error bars represent the SEM of mCherry levels from three experiments over three days (**b-c**) or a single day (**d**).



733

734 **Figure 6.** Validating the LPA with mammalian cells by spatial patterning of transgene
735 delivery with PHYB/VNP-PIF6. **(a)** PHYB/VNP-PIF6 system. **(b)** HeLa cells expressing
736 PhyB(908)-NLS were treated with 15 μM PCB and VNP-PIF6 (2,000 viruses per cell) and
737 exposed through a photomask (top row and **Supplementary Fig. 17b**) to 2.0 $\mu\text{mol m}^{-2} \text{s}^{-1}$
738 far-red for 30 min followed by 1.0 $\mu\text{mol m}^{-2} \text{s}^{-1}$ far-red and variable red intensities (shown
739 in $\mu\text{mol m}^{-2} \text{s}^{-1}$ in upper left of cell fluorescence images) for 60 min. Image corresponding
740 to red intensity of 1.75 $\mu\text{mol m}^{-2} \text{s}^{-1}$ was acquired with photomultiplier setting of 80 while
741 all others were acquired with photomultiplier setting of 60. **(c)** Contrast ratio of cell
742 fluorescence patterns from images in panel b (bottom row). Symbols represent the
743 average ratio of pixel intensity in three light-exposed regions to an unexposed region,
744 while error bars represent the SEM.



745

746 **Figure 7.** Validating the LPA with cyanobacteria by entraining circadian rhythm in *S.*
747 *elongatus*. (a) Schematic representation of entrainment protocol. Cells grown under
748 constant light were placed in the LPA and entrained with three light-dark cycles, with dark
749 periods starting at different times in order to shift the phases of each well. The cells were
750 then transferred to a plate reader for measurement of luminescence under constant light.
751 (b) Luminescence oscillation for cultures entrained starting at different times. Cultures
752 were entrained starting at zero (red), four (orange), eight (yellow), 12 (green), 16 (blue)
753 and 20 (purple) hours. Fits of raw data were normalized to equalize peak height, and the
754 normalized fits were averaged across three replicates except for the cultures in yellow for
755 which only two replicates could be obtained. Bars indicate SEM. (c) Phase of cultures
756 entrained starting at different times. Colors are the same as in b. Dots indicate cosine
757 acrophase (phase of peak) of the replicates. Lines indicate the best fit for the expected
758 locations of acrophase for perfect entrainment.